Engineering Science and Technology, an International Journal 62 (2025) 101975

Contents lists available at ScienceDirect

Engineering Science and Technology, an International Journal

journal homepage: www.elsevier.com/locate/jestch

Enhanced sensing capabilities of UV–visible *p-n* and *p-i-n* photodiodes using unique layer and contact configurations

Ahmed Ali Alarabi [a], Osman Çiçek [b,*], Hasan Makara [a], Fatih Ünal [c], Merve Zurnacı [d], Şemsettin Altındal [e]

[a] Department of Metallurgy and Materials Engineering, Kastamonu University 37100 Kastamonu, Turkey
[b] Department of Electrical-Electronic Engineering, Faculty of Engineering and Architecture, Kastamonu University 37150 Kastamonu, Turkey
[c] Central Research Laboratory, Application and Research Center, Giresun University, Giresun, Turkey
[d] Central Research Laboratory, Kastamonu University, Kastamonu, Turkey
[e] Department of Physics, Faculty of Sciences, Gazi University 06560 Ankara, Turkey

ARTICLE INFO

Keywords:
Photodiodes
Organic semiconductor
Self-powered mode
Photosensitivity
Electronic Properties

ABSTRACT

This paper focuses on the ultraviolet–visible (UV–vis) light response of the p-n and p-i-n vertical self-powered photodiodes (PDs) based on p-PMItz/n-Si, p-PMItz/n-4HSiC and p-PMItz/i-SiO_2/n-Si Heterojunctions. The PDs, referred to as Device A-B-C-D-E and F according to the modified structures, were produced to increase the sensing capacity using distinct anode contacts. The basic fundamental parameters were recorded using the I-V data of PDs with thermionic emission theory (TE) and Ohm's law. The results showed that, in line with the literature, the potential barrier height (Φ_{Bo}) decreased, and the ideality factor (n) increased with increasing illumination intensity. Additionally, the voltage-dependent series resistances (R_s) of PDs in the dark and under different UV–vis light intensities were determined using Ohm's laws. It was recorded that R_s decreased as light intensity increased. On the other hand, the photosensitivity properties of PDs in UV–vis intensities depending on the voltage were investigated. The photosensitivity of the fabricated Device B reached a maximum of $4.05x10^4$ at short circuit voltage (V_{sc} = 0 V). In contrast, when self-powered, the short-circuit voltage (V_{oc}) showed better photosensitivity (with a minimum of 0.058). Additionally, the specific detectivity (D*) and the responsivity (R) of the PDs were calculated. According to the literature, the R and D* decreased with increasing power density at zero-bias voltage. Also, the R of Device B is higher, and D* is lower than other devices. The linear dynamic range (LDR) of Device A reaches ~ 92 dB with maximum (V_{bias} = 0 V) while the dark current is 0.038 nA with minimum (in self-powered mode). Device B is considered suitable for the PDs (in self-powered mode) among other devices.

1. Introduction

Nowadays, photodiodes (PDs) bearing on *p-n* and *p-i-n* junctions are of critical importance in various fields such as flame detection, detection of UV rays, monitoring of biological agents, missile threat warning systems, providing low bit error rates and secure data transmission [1]. Advances in organic semiconductors and *p-n* and *p-i-n* junctions are associated with the evolution of hybrid organic/inorganic semiconductor heterojunctions that can enhance the potential of all-organic or inorganic junctions; these hybrid structures can play an essential role in the development of optoelectronic and electronic applications [2,3]. Additionally, organic semiconductors are flexible materials that can find use in a wide range of technologies, such as transistors, solar cells, OLEDs, and especially sensors, and have the potential to cope with low current densities and charge injection losses in electrically driven organic lasers [4,5]. It is essential to improve the performance of devices by optimizing the properties of organic and hybrid semiconductor *p-n* and *p-i-n* junctions, which is the aim of most research nowadays [6–8].

Generally, an external power source is applied to prevent photo-generated electron-hole (e^-/h^+) pairs from recombining for a photo response. Theoretically, both the p-n and p-i-n type PDs, when photons whose energy is higher than the bandgap energy ($E = hc/q\lambda$) are exposed on or near the junction of them, e^-/h^+ pairs can be created at the junction. In the reverse bias region, the interior and external electric

* Corresponding author.
E-mail address: ocicek@kastamonu.edu.tr (O. Çiçek).

https://doi.org/10.1016/j.jestch.2025.101975
Received 17 October 2024; Received in revised form 26 December 2024; Accepted 23 January 2025
Available online 28 January 2025

fields (ε, E)) have the same direction, and so they prevent the recombination of these e^-/h^+ pairs. Thus, the energy of photons is converted into DC electricity. this phenomenon is called the photovoltaic event, and the resulting current is called photocurrent. In general, the magnitude of photocurrent is quite higher in the reverse bias region when compared to the positive bias region. Because in the reverse bias voltage, the ε and E electric fields are in the same direction, while in forward biases, they are in the opposite direction, and therefore, the total electric field becomes smaller. On the other hand, this approach is that e^-/h^+ charges originating from ionized donors and acceptors in *n*-type and *p*-type organic semiconductors come together with both *n*-type and *p*-type semiconductors to form a complex *i*-layer. [2,3,9]. The critical point of enhancing semiconductors in complex multi-junctions is mobility in vertical and lateral directions. This is obtained by creating structural order through band-like charge mobility, organic polycrystals, and single crystals and maximizing charge carrier mobility [9,10]. On the same line, different constrictions of organic semiconductors can be built among them *p-n*, *p-i-n*, and especially Schottky diodes, and each of these diodes serves a specific function. This leads to more research investigating multi-junction-based applications on organic semiconductors, characterized by organic semiconductors grown on inorganic wafers [10,11]. Given that Si is well-known in literature and abundant material worldwide, the fabrication of these based multiple junctions is critical in determining the fundamental diode properties of the deposited thin film layer. Therefore, developing Si semiconductors for subsequent applications will be essential in achieving high device performance [4,5].

Most PDs made using inorganic semiconductors are operated in reverse biased or self-powered modes, followed by monitoring the current flow following the changes in light intensity. These PDs show good stability, high photonic response, and low binding energy to the exactions (photo-generated bonding of e^-/h^+) [4,11]. Herein, many e^-/h^+ pairs are generated in the depletion layer or at the junction, and some holes are trapped because of their smaller mobility [7,8]. However, the high energy requirement and complex mechanisms involved in inorganic semiconductors' production and purification processes limit the application areas of PDs based on inorganic semiconductors. On the other hand, organic semiconductors employed in PD applications have drawn much interest because they are especially well-suited for wide-area image detectors, offer economical production methods involving low-temperature processes, and can be applied to flexible and lightweight surfaces. Furthermore, their optoelectronic properties can be interestingly altered in the material and device stages [4].

Self-powered PDs are divided into three types (according to their structures): *p-n* homojunction, Schottky junction, and heterojunction. The term self-powering generally means that devices control or draw the energy they need to operate from the system, so they do not require an external power source (such as electricity) [12,13]. Self-powered PDs are similar to solar cells in that current is generated by e^-/h^+ pair separation, thanks to a built-in voltage in the depletion region of *p-n* junctions [13]. The difference is that while self-powered PDs detect incoming light, the solar panel produces electricity. Organic semiconductors are especially suitable for self-powered UV PDs containing *p–n* heterojunctions. The large internal electric field can be formed by arranging the energy level of *n*-type and *p*-type semiconductors, thus exhibiting excellent performances for PDs. However, the performance of UV PDs with self-powered heterojunctions is insufficient for practical applications. Various approaches have been developed to increase the production of photogenerated carriers, the efficiency of interface separation, and the transfer of carriers, thereby improving the performance of heterojunction UV PDs. One approach envisages appropriately designing semiconductors' energy band structure to enhance photogenerated carriers' separation capacity.

A thorough and comprehensive literature review revealed some optic, fluorescence, and optoelectronic properties of phenanthroimidazole bearing derivative (PMItz) as a *p*-type organic semiconductor [14]. Using a new and different organic layer (p-PMItz) can alter the performance of p-n and p-i-n structures, thus offering an attractive alternative to traditional inorganic PDs in device applications. The effect is evident in the characteristics when choosing the *p*-PMItz organic layer as a semiconductor. In (indium) and Ag (silver) contacts were used for the anode, and Al (aluminum) contacts were used for the cathode. Therefore, we use various heterojunction arrangements to illustrate some characteristics of vertical PDs *p-n* and *p-i-n* with the *p*-PMItz organic semiconductor.

2. Experimental details

To explore these advancements, we conducted a series of experiments focusing on the unique configurations of *p-n* and *p-i-n* PDs.

2.1. Fabrications of p-n and p-i-n structures with Ag and In anode electrodes

n-Si (P-doped/*Resistivity:*1–10 Ω.cm, (111)), *i*-SiO_2/n^{++}-Si (P-doped/*Resistivity:* 0.001–0.005 Ω.cm, (100)) and *n*-4HSiC (*Resistivity:* 0.015–0.03 Ω.cm) substrates were exposed to a soapy water solution for 10 min in an ultrasonic bath. The substrates were removed from the solution and rinsed thoroughly with DI water. For the *i*-SiO_2/*n*-Si substrate, no extra cleaning was applied. also, the surface was dried with The *n*-Si and *n*-4HSiC substrates were taken into a beaker (glass), and acetone was added and then kept in an ultrasonic bath (10 min). After cleaning with acetone, *n*-Si and *n*-4HSiC substrates were placed in a beaker with propanol and kept in an ultrasonic bath (10 min). The surfaces of *n*-Si and *n*-4HSiC were cleaned using propanol and then dried with N_2(g). After cleaning, a layer of high purity (99.999 %) 150 nm thick Al is grown in the high vacuum physical vapor deposition (PVD) system completely behind the *n*-Si, *i*-SiO_2/*n*-Si and *n*-4HSiC substrates at about 26 °C and $1.9x10^{-5}$ Torr pressure. To form an ohmic/cathode contact for low resistances, *n*-Si/Al, *i*-SiO_2/*n*-Si/Al, and *n*-4HSiC/Al were annealed at 500 °C in N_2 for 10 min. On the other hand, the PVD method was used to deposit *p*-PMItz as a thin film on substrates at about 21 °C and $4.9x10^{-6}$ Torr pressure. Finally, dots of high-purity Ag and In with a thickness of 150 nm were physically evaporated onto the organic layer in 1 mm dots. The PVD system was used to grow the rectifier contacts. The devices have been completed exactly as illustrated in Fig. 1.

2.2. Structural Analysis of p-PMItz films

Fig. 2 presents the SEM images used to evaluate the surfaces and thicknesses of the *p*-PMItz layers. The PVD method was used to deposit *p*-PMItz as a thin film on substrates with near thicknesses of 550 nm, 350 nm, 750 nm, 330 nm, 450 nm, and 460 nm, as shown in Fig. 2, respectively. The surfaces of the *p*-PMItz films are dense and homogeneous.

2.3. Optical Band Gap of p-PMItz

The $(\alpha h\nu)^2$-$(h\nu)$ plot is presented for the band gap of p-PMITz. For this, absorption measurements of *p*-PMItz were used. The graph *p*-PMItz $(\alpha h\nu)^2 - (h\nu)$ is given in Fig. 3. According to the data obtained from the graph, the optical band gap (*Eg*) was calculated as 3.02 eV.

2.4. Measurement of vertical self-powered photodiodes

Electrical properties were carried out by a Keitley 2400 current voltage source meter and a Scientech SF300A solar simulator via a microcomputer and an IEEE-488 AC/DC converter board (Fig. 4).

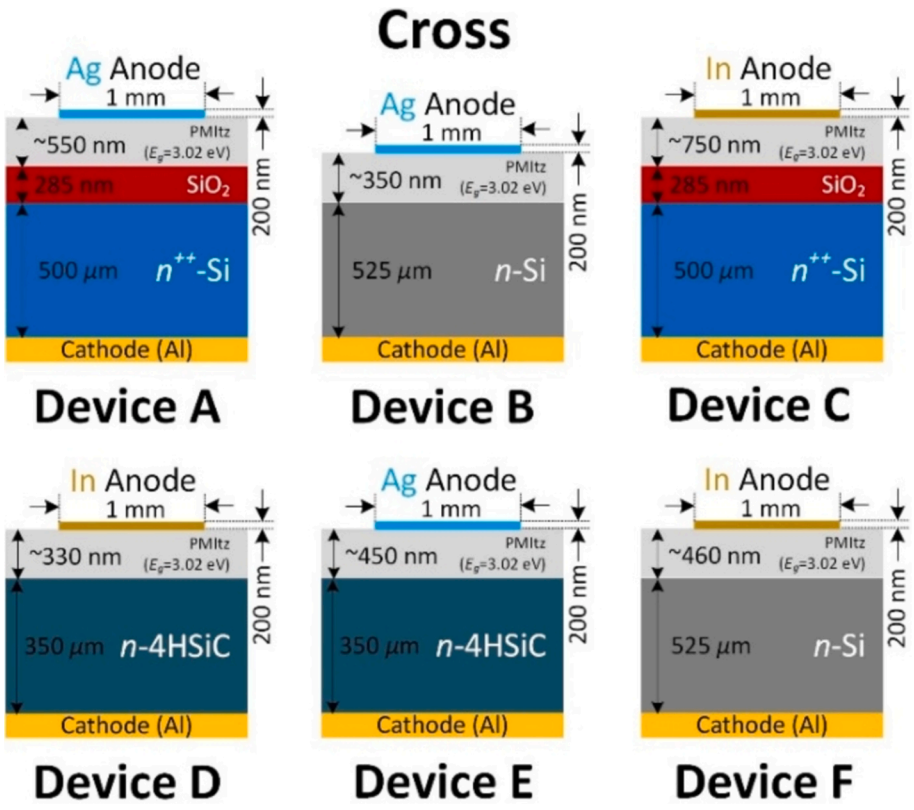

Fig. 1. Schematic of Vertical Self-Powered Photodiodes based on *p*-PMItz/*n*-Si, *p*-PMItz/*n*-4HSiC and *p*-PMItz/*i*-SiO_2/*n*-Si Heterojunctions.

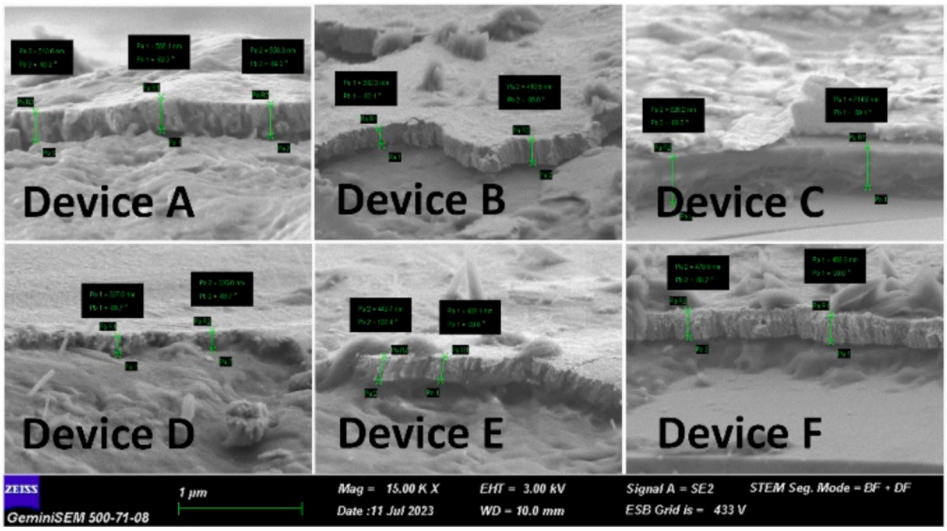

Fig. 2. SEM images of the *p*-PMItz films.

3. Results and discussion

3.1. Main characteristics of the PDs

The electronic parameters of devices, such as ideality factor (n), potential barrier height (Φ_{Bo}), parallel resistance (R_{sh}), and series resistance (R_s), can be calculated using various theorems. These theorems, including the thermionic emission theory (TE), Ohm's law, and Cheung and Cheung's method, are reliable and can obtain accurate results [13,15]. They also make it easier to compare different calculations with each other.

Fig. 5 displays the current–voltage characteristics of the devices. It includes semi-logarithmic forward and reverse bias voltage plots, the change of darkness, and UV–vis light intensities. Herein, it can be concluded that the devices exhibit a rectifier behavior. As well-known as the behavior of a photodiode, the forward and reverse current values at ± 3 V also increase with light intensity, providing further evidence. In all devices, I-V curves exhibit asymmetric behavior and electrical conductivity changes with increasing light intensity. This is important for the PDs applications [16,17].

Under dark, the rectification ratio (RR) values of Ag/PMItz/SiO_2/n^{++}-Si (Device A) and In/PMItz/SiO_2/n^{++}-Si (Device C) at 3 V were

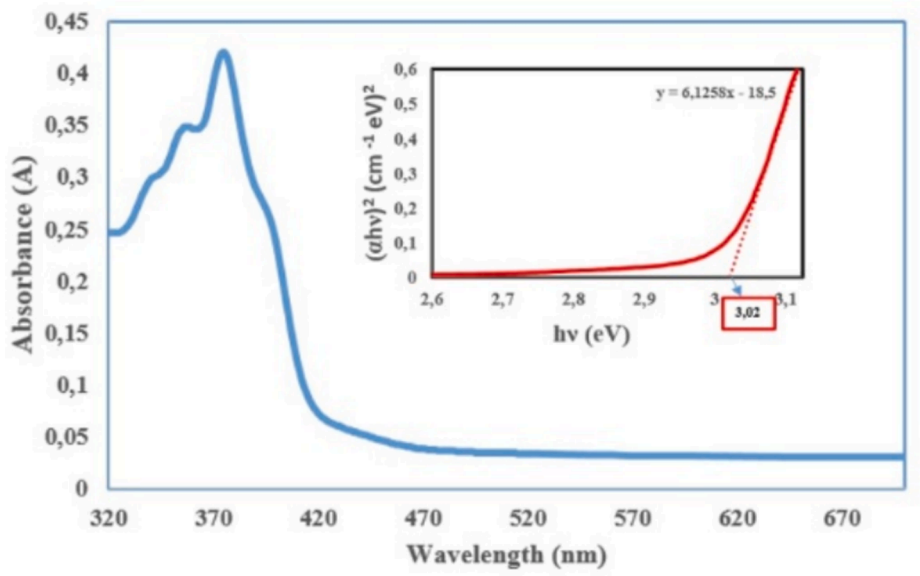

Fig. 3. Absorption spectrum and optical band gap of the *p*-PMItz film.

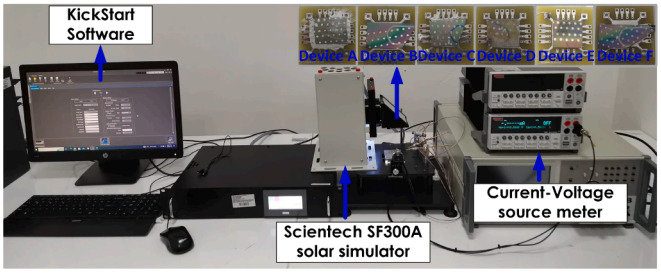

Fig. 4. Experimental setup for vertical self-powered photodiodes.

$1.36x10^{01}$ and $5.55x10^{00}$ for *p-i-n* structures, respectively. Ag/PMItz/n-Si (Device B) and In/PMItz/n-Si (Device F) values are $1.63x10^{03}$ and $6.7x10^{01}$ for Si-based *p-n* structures, respectively. The values of In/PMItz/*n*-4HSiC (Device D) and Ag/PMItz/*n*-4HSiC (Device E) are $7.83x10^{04}$ and $7.94x10^{04}$, for SiC-based *p-n* structures, respectively. The RR values of the devices using Ag metal contact are higher than those with In metal contact. The different work functions of metals can explain this. While the work function for Ag is 4.26 eV, it for In metal is 4.12 eV [18,19].

It is also observed that the RR values of *p-n* devices fabricated with different metals in the same junction are higher than the devices' values with metals having low work function. It was observed that the RR value of Device C was lower than all of them. This can be attributed to the interface's increased charge, especially in the forward voltage region [20,21].

The RR value of Device E is relatively high compared to the literature [22–24]. This high value is caused by reverse saturation current and is essential for the PDs [25]. On the other hand, the RR values of all devices generally decreased with increasing light intensity. The reason for this decrease is the increasing current in the reverse bias region. It is also an expected behavior in PDs [26]. Despite having a high RR, the devices with *n*-4HSiC substrates have low sensitivity according to light intensity. Nevertheless, to accurately calculate their electronic parameters related to the sensitivity of the devices, TE and Ohm's law still need to be applied.

According to the theory of TE, the expression for the current in a metal–semiconductor structure containing the interface layer-series resistance is as follows [13,15]:

$$I = I_o\left[exp\left(\frac{q(V-IR_s)}{nkT}\right)-1\right] \quad (1)$$

where,

$$I_o = AA^*T^2exp\left(-\frac{q\phi_{Bo}}{kT}\right) \quad (2)$$

The variables in the equations are q, which is the electron charge ($1.6x10^{-19}$C); T, which is the absolute temperature (Kelvin); V, which is the applied voltage; IR_s, which is the voltage drop across R_s; k, which is the Boltzmann constant ($1.38x10^{-23}JK^{-1}$); I_o, which is the saturation current, is obtained from the intersection of a straight line $\ell n(I)$ at V_{bias} = 0 V; A is the rectifier contact area; A^* is the Richardson constant, which equals to 112 $Acm^{-2}K^{-2}$ and 148.8 $Acm^{-2}K^{-2}$ for *n-type* Si and *n*-type 4H-SiC, respectively; n, which is the ideality factor deduced by Eq. (1); and Φ_{Bo}, which is the potential barrier height calculated by Eqs (3) and (4) [13,15].

$$\phi_{Bo} = \frac{kT}{q}\ell n\left(\frac{AA^*T^2}{I_o}\right) \quad (3)$$

$$n = \frac{q}{kT}\left[\frac{d(V-IR_s)}{d(\ell nI)}\right] \quad (4)$$

Table 1 shows the experimental for I_o, n, Φ_{Bo}, R_{sh}, and R_s. With increased UV–vis light intensity, n values increase, and Φ_{Bo} values decrease. These results are consistent with the literature [27]. Under dark, Φ_{Bo} values range from 0.73 to 0.87 eV, and n values range from 2.69 to 4.20. The highest Φ_{Bo} value was observed in Device E, while the lowest Φ_{Bo} value was observed in Device F. Although the lowest n value is observed in Device B, these values are more significant than unity, indicating that the devices are not ideal. The n value exceeding unity in fabricated devices is often due to various inhomogeneities at the interface, including variability in material composition, surface roughness, and the presence of defects or dislocations that trap carriers [28]. Additional factors such as oxidation and contamination, temperature gradients during fabrication, atomic interface roughness, mechanical stress, and irregular doping concentrations also contribute to these inconsistencies. [15].

The I_o values of the devices in the dark range from $9.57x10^{-11}$ to $1.72x10^{-08}$ A. The highest I_o value was observed in Device F, and the lowest I_o value was observed in Device E. In all devices, I_o values

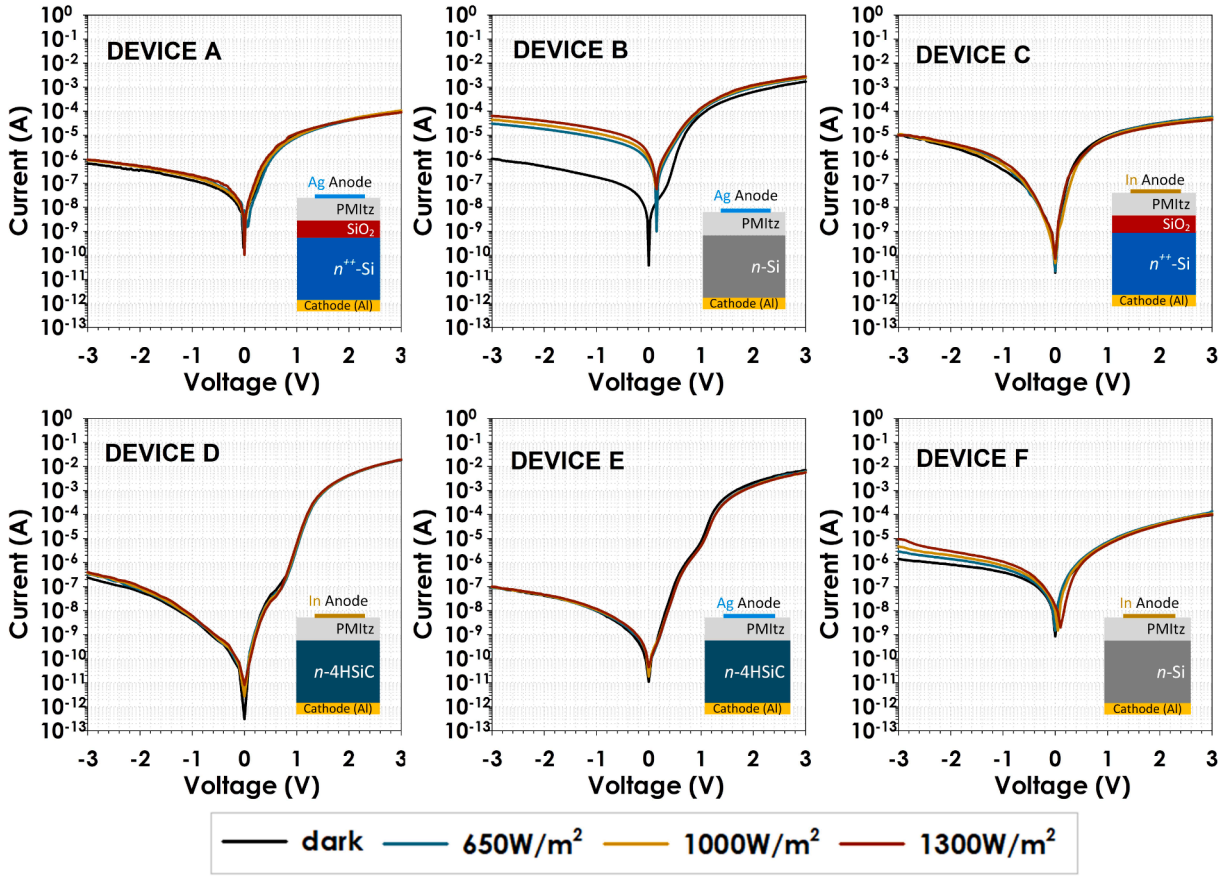

Fig. 5. The devices' current–voltage characteristics in dependence on UV–vis light intensities.

increased due to the increase in minority carriers with increasing light intensity. Moreover, according to the correlation between I_o and Φ_{Bo}, this situation rises with decreasing Φ_{Bo}.

R_s and R_{sh} are essential parameters in *p-n* junctions or other *p-i-n*, MOS, and MS structures and are also expected to be small and high for device performance, respectively. Based on the *I-V* characteristic, the resistance values are determined by the formula $R_i = dV/dI$. R_i has two combinations and gives R_s value under forward bias and R_{sh} under reverse bias [15]. In the dark, the R_s values range from 0.16 to 33.45 kΩ, while the R_{sh} values range from 0.29 to 33.88 MΩ. While no meaningful change was observed in R_s values with increasing light intensity, R_{sh} values decreased. R_{sh} values are almost 10^3 times larger than R_s values and are acceptable for PDs applications. It was observed that the devices, according to their R_s and R_{sh} values, used Ag metal contact and exhibited more than those with In metal contact.

3.2. The self-powered mode

The self-powered mode in PDs operates without an external power supply (V_{bias} = 0 V), offering several advantages such as simplicity in circuit design, low power consumption, and high photosensitivity (PS). This mode eliminates the need for a separate voltage source, reducing system complexity and size, which is particularly beneficial for battery-operated or energy-harvesting devices. Additionally, self-powered PDs minimize noise that could potentially affect signal quality and facilitate easier integration into compact systems. They are versatile for use in optical communications, light sensing, and environmental monitoring, making them cost-effective solutions for various applications. Herein, additionally, it is essential to determine the PS properties of the PDs depending on the UV–vis light intensities. The light-to-current conversion quality can also be found for PD applications by calculating the photocurrent-to-dark current ratio (I_{ph}/I_d). Fig. 6 shows the graphs of the PS values of the devices produced at 650, 1000, and 1300 W/m^2 light intensities in the range of ± 3 V.

The performance of various devices under different conditions can be summarized as follows: Device A exhibits PS values of 3.68, 4.83, and 6.46 at −3 V, and 1.07, 1.12, and 1.44 at 3 V with increasing light intensities, achieving maximum PS values in self-powered mode (0 V) of 27.1, 24.3, and 22.8. Device B shows significantly higher PS values of 28.9, 42.5, and 61.0 at −3 V and 1.4, 1.47, and 1.65 at 3 V, with maximum PS values in self-powered mode of 18700, 27000, and 40500. In contrast, Device C's PS values are lower, at 1.05, 1.01, and 0.96 at −3 V, and 0.995, 0.879, and 0.755 at 3 V, with maximum PS values in the self-powered mode of 1.14, 2.52, and 3.81. Device D displays PS values of 1.40, 1.53, and 1.69 at −3 V, and 1.02, 1.04, and 1.04 at 3 V, reaching maximum PS values of 12.3, 18.8, and 26.8 in self-powered mode. Device E's PS values are 1.01, 1.09, and 1.13 at −3 V, and 0.87, 0.82, and 0.80 at 3 V, with maximum values of 3.27, 1.66, and 4.00 when self-powered. Finally, Device F shows PS values of 2.01, 3.27, and 6.68 at −3 V, and 1.43, 1.14, and 1.05 at 3 V, with maximum self-powered PS values of 1.72, 11.0, and 18.8. In all devices, it was observed that the PS values at reverse bias were higher than the PS values at forward bias. This is an expected behavior for PDs. The maximum PS values for all devices were observed in self-powered mode (0 V).

In general, it was observed that the PS values increased in the reverse bias with increasing light intensity. The lowest PS value was found in Device E; the highest PS value was found in Device B. When comparing the PS values of devices with *n*-Si substrates, it was found that Device B with Ag rectifier contact performs better than Device F.

Additional important parameters utilized in the test validity and detection properties of PDs were determined as specific detectivity (D^*) and responsivity (R), which are represented by the following equations

Table 1
The calculated electronic parameters of the devices.

Device	Power (W/m^2)	from *TE*			from *Ohm's Law*		
		I_o (A)	**n**	**Φ_{Bo} (eV)**	**R_{sh} (MΩ) at −3V**	**R_s (kΩ) at 3 V**	**RR**
DEVICE A	0	3.46×10^{-9}	3.00	0.77	4.54	33.45	1.36×10^{01}
	650	5.45×10^{-09}	3.85	0.76	3.27	33.83	0.97×10^{01}
	1000	1.11×10^{-08}	3.98	0.74	3.26	28.26	1.15×10^{01}
	1300	2.24×10^{-08}	4.25	0.72	3.12	33.68	0.92×10^{01}
DEVICE B	0	6.09×10^{-10}	2.69	0.81	2.89	1.77	1.63×10^{03}
	650	8.34×10^{-08}	4.83	0.69	0.10	1.26	7.93×10^{01}
	1000	1.37×10^{-07}	5.06	0.68	0.07	1.20	5.66×10^{01}
	1300	1.62×10^{-07}	5.10	0.67	0.05	1.07	4.41×10^{01}
DEVICE C	0	3.37×10^{-9}	2.82	0.77	0.29	51.64	5.55×10^{00}
	650	4.06×10^{-09}	3.66	0.76	0.27	51.90	5.25×10^{00}
	1000	7.87×10^{-09}	4.23	0.75	0.28	58.77	4.81×10^{00}
	1300	1.19×10^{-08}	4.48	0.74	0.29	72.12	4×10^{00}
DEVICE D	0	2.81×10^{-10}	4.14	0.84	12.63	0.16	7.83×10^{04}
	650	3.35×10^{-10}	4.64	0.83	9.03	0.16	5.70×10^{04}
	1000	4.12×10^{-10}	4.79	0.83	8.24	0.16	5.30×10^{04}
	1300	3.73×10^{-10}	4.84	0.83	7.48	0.15	4.85×10^{04}
DEVICE E	0	9.57×10^{-11}	2.79	0.87	33.88	0.43	7.94×10^{04}
	650	9.65×10^{-11}	3.08	0.87	33.68	0.49	6.87×10^{04}
	1000	1.16×10^{-10}	3.13	0.86	31.16	0.52	5.99×10^{04}
	1300	1.35×10^{-10}	3.21	0.86	30.00	0.54	5.59×10^{04}
DEVICE F	0	1.72×10^{-08}	4.20	0.73	2.11	31.48	6.7×10^{01}
	650	7.99×10^{-08}	7.01	0.69	1.05	21.97	4.8×10^{01}
	1000	8.45×10^{-08}	7.87	0.69	0.64	27.64	2.3×10^{01}
	1300	9.76×10^{-08}	8.66	0.69	0.32	29.93	1.1×10^{01}

[30].

$$R = \frac{I_{ph} - I_d}{AP} \tag{5}$$

$$D* = \frac{R\sqrt{A}}{\sqrt{2qI_d}} \tag{6}$$

Here, the D^* formulation relates the R, the area A of the PD, the electron charge q equals to 1.6×10^{-19} C, and the dark current I_d [30]. The graphs of the devices' changes in the R and D^* versus the range of ± 3 V at 650, 1000, and 1300 W/m^2 light intensities are displayed in Fig. 7.

Devices A, B, C, D, E, and F exhibit various R values in response to increasing light intensities. At −3 V, Device A's R values are 5.05 × 10–5, 5.07 × 10–5, and 5.92 × 10–5 (A/W). At 3 V, these values change from an average of approximately 5.68 × 10–5 to 1.97 × 10–4, 32.2 × 10–4, and 1.23 × 10–4 (A/W). Device B shows R values of 2.30 × 10–2, 2.74 × 10–2, and 3.31 × 10–2 (A/W) at −3 V, changing to 0.54, 0.51, and 0.59 (A/W) at 3 V. Device C has values of 10.3 × 10–5, 1.78 × 10–5, and 3.83 × 10–5 (A/W) at −3 V and changes from these to 5.7 × 10–5, 89.8 × 10–5, and 139.3 × 10–5 (A/W) at 3 V. Device D presents values of 7.24×10^{-6}, 8.72×10^{-6}, and 1.6 × 10–5 (A/W) at −3 V, changing to 6.34 × 10–2, 8.79 × 10–2, and 7.95 × 10–2 (A/W) at 3 V. Device E displays R values of 1.43×10^{-8}, 5.41×10^{-7}, and 1.97×10^{-7} (A/W) at −3 V, which change to 0.13, 0.1, and 0.11 (A/W) at 3 V. Lastly, Device F reports R values of 2.27 × 10–4, 3.22 × 10–4, and 5.15 × 10–4 (A/W) at −3 V, changing to 1.23 × 10–2, 3.45 × 10–3, and 2.73 × 10–3 (A/W) at 3 V.

The R values increased with increasing the voltage under both forward and reverse biases. While increasing light intensity, the R values of devices A, B, D, and F increased in the reverse bias, but the R values of devices C and E decreased. This can be explained by the decrease in absorption with radial variation of light intensity [31]. This phenomenon was also observed in some devices under forward bias. The highest R value was observed in device B in both forward and reverse biases.

Device F's D^* values are $3.37x10^8$, $4.78x10^8$, $7.63x10^8$ (Jones) at −3 V, while they are also $2.23x10^9$, $6.26x10^8$ and $4.94x10^8$ (Jones) at 3 V with increasing light intensities, respectively.

The device performance in terms of the D^* under varying conditions is as follows: Device A shows D^* values of $2.63x10^7$, $3.16x10^7$, and $5.80x10^7$ (Jones) at −3 V, and $8.21x10^8$, $1.14x10^8$, and $1.03x10^9$ (Jones) at 3 V with increasing light intensities. Device B exhibits significantly higher D* values of 4.00x101°, 4.76x101°, and 5.74x101° (Jones) at −3 V, decreasing to 2.33x101°, 2.20x101°, and 2.52x101° (Jones) at 3 V. Device C's D* values are lower, recorded at $5.61x10^7$, $9.70x10^6$, and $2.09x10^7$ (Jones) at −3 V, and increasing to $1.32x10^7$, $2.08x10^8$, and $3.23x10^8$ (Jones) at 3 V. Device D shares the same D* values as Device A at −3 V ($2.63x10^7$, $3.16x10^7$, and $5.80x10^7$) and similarly responds at 3 V with values of $8.21x10^8$, $1.14x10^9$, and $1.03x10^9$ (Jones). Device E demonstrates lower sensitivity at −3 V with D* values of 8.52x104, $3.21x10^6$, and $1.17x10^6$ (Jones), but significant values at 3 V of $2.64x10^9$, $2.11x10^9$, and $2.23x10^9$ (Jones). Lastly, Device F shows strong performance with D* values of $3.37x10^8$, $4.78x10^8$, and $7.63x10^8$ (Jones) at −3 V, and values of $2.23x10^9$, $6.26x10^8$, and $4.94x10^8$ (Jones) at 3 V with increasing light intensities. The highest D^* values were observed in Device B under both forward and reverse biases. D^* values in reverse bias increased except for Device C, which increased in light intensity. In forward bias, a similar situation was observed except for Device E and F. This can be explained by e^-/h^+ recombination.

Fig. 8 shows the variations of I_{ph}, R, D^* and signal to noise ratio (LDR (dB) = $20\log(I_{ph}/I_d)$) values of the fabricated devices in self-powered mode (0 V) depending on the light intensity.

In Fig. 8a, the I_{ph} values of the devices are the range from 7.35 to 0.104nA for Device A, the range from 708.8 to 1535.2nA for Device B, the range from 0.022 to 0.072nA for Device C, the range from 0.00037 to 0.00081nA for Device D, the range from 0.037 to 0.044nA for Device E, the range from 1.46 to 15.97nA for Device F with changing light intensity, at self-powered mode (V = 0 V), respectively. The I_{ph} values of all devices except Device A increased with increasing light intensity. The change in current values without any external excitation potential means that the produced devices can operate in self-powered mode.

The increase in I_{ph} values can be explained by the existence of e^-/h^+ pairs depending on the light intensity and the increase in photo-carriers. In contrast, the situation at Device A can be explained by recombination [32].

In Fig. 8b, the R values of the devices are the range from 1.43 to 0.003 μA/W for Device A, the range from 130.18 to 150.43 μA/W for

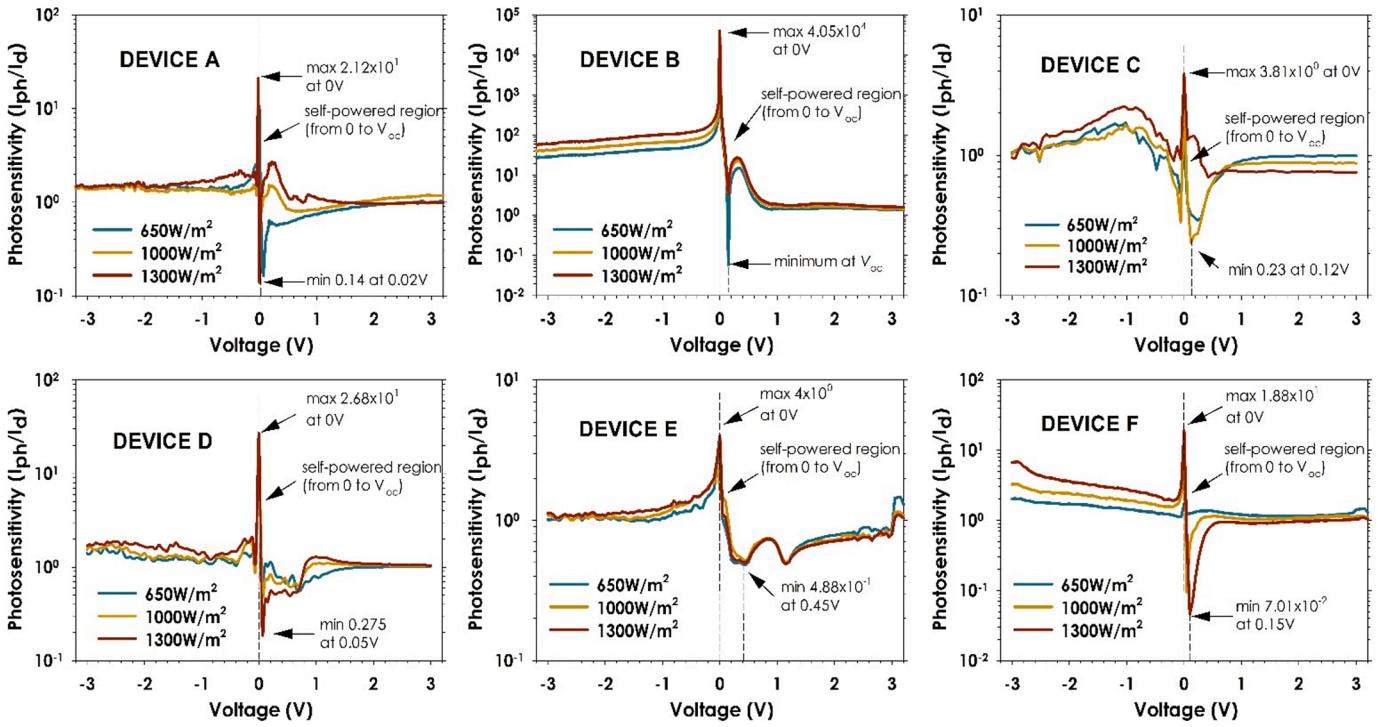

Fig. 6. The photosensitivity characteristics of the PDs under UV–vis light conditions.

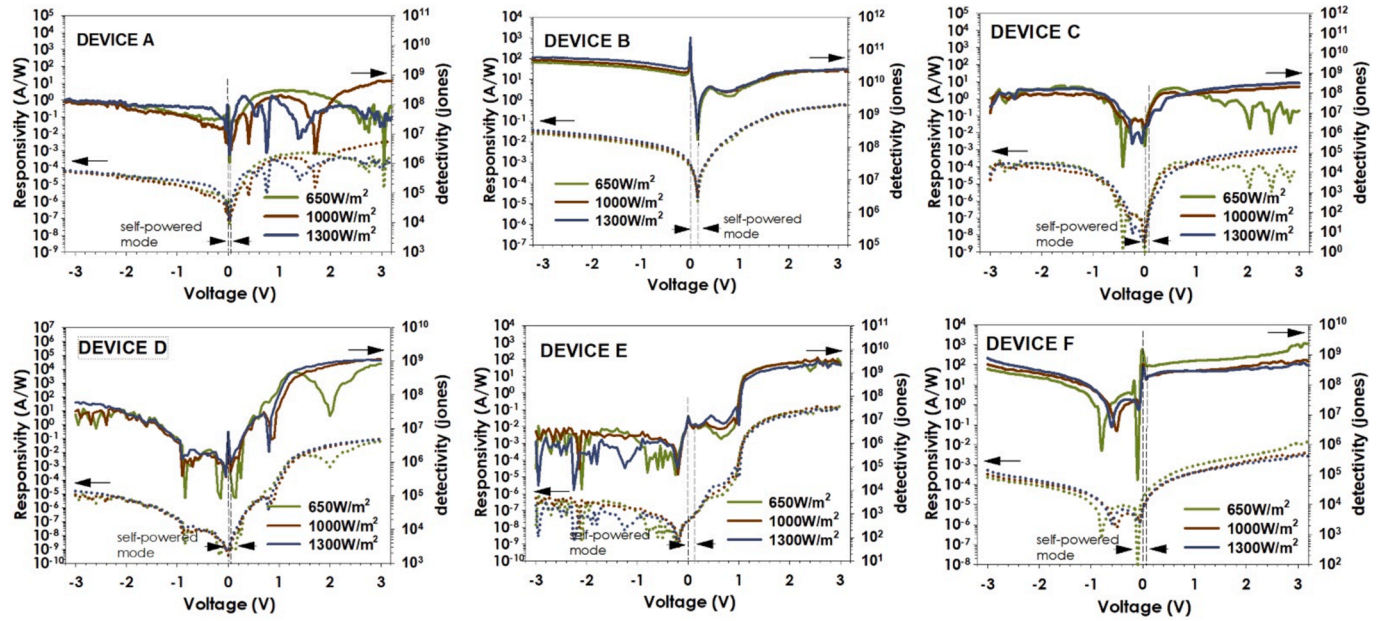

Fig. 7. The responsivity and detectivity characteristics of the PDs under UV–vis light conditions.

Device B, the range from 0.0037 to 0.0052 μA/W for Device C, the range from 0.000067 to 0.000077 μA/W for Device D, the range from 0.00092 to 0.0049 μA/W for Device E, the range from 0.119 to 1.48 μA/W for Device F with changing light intensity, at self-powered mode ($V = 0$ V), respectively. The highest R values were observed in Device B and the lowest R values were observed in Device D.

In Fig. 8c, the D^* values of the devices are the range from $2.9\text{x}10^8$ to $5.8\text{x}10^5$ Jones for Device A, the range from $3.74\text{x}10^{10}$ to $4.32\text{x}10^{10}$ Jones for Device B, the range from $2.14\text{x}10^5$ to $2.12\text{x}10^6$ Jones for Device C, the range from $6.82\text{x}10^5$ to $7.79\text{x}10^5$ Jones for Device D, the range from $4.92\text{x}10^5$ to $2.61\text{x}10^6$ Jones for Device E, the range from $7.25\text{x}10^6$ to $8.99\text{x}10^7$ Jones for Device F with changing light intensity, at self-powered mode ($V = 0$ V), respectively. The highest R was found in Device B, and the lowest R was found in Device D. Similar to I_{ph} and R values, the highest D^* value was observed in Device B.

In Fig. 8d, the *LDR* values of the devices are the range from $3.98\text{x}10^1$ to $2.83\text{x}10^0$ dB for Device A, the range from $8.54\text{x}10^1$ to $9.21\text{x}10^1$ dB for Device B, the range from $1.15\text{x}10^0$ to $8.03\text{x}10^0$ dB for Device C, the range from $2.18\text{x}10^1$ to $2.86\text{x}10^1$ dB for Device D, the range from $4.4\text{x}10^0$ to $1.20\text{x}10^1$ dB for Device E, the range from $4.7\text{x}10^0$ to $2.55\text{x}10^1$ dB for Device F with changing light intensity, at self-powered mode ($V =$ 0 V), respectively. The dark current values are 0.0753, 0.0379, 0.0189,

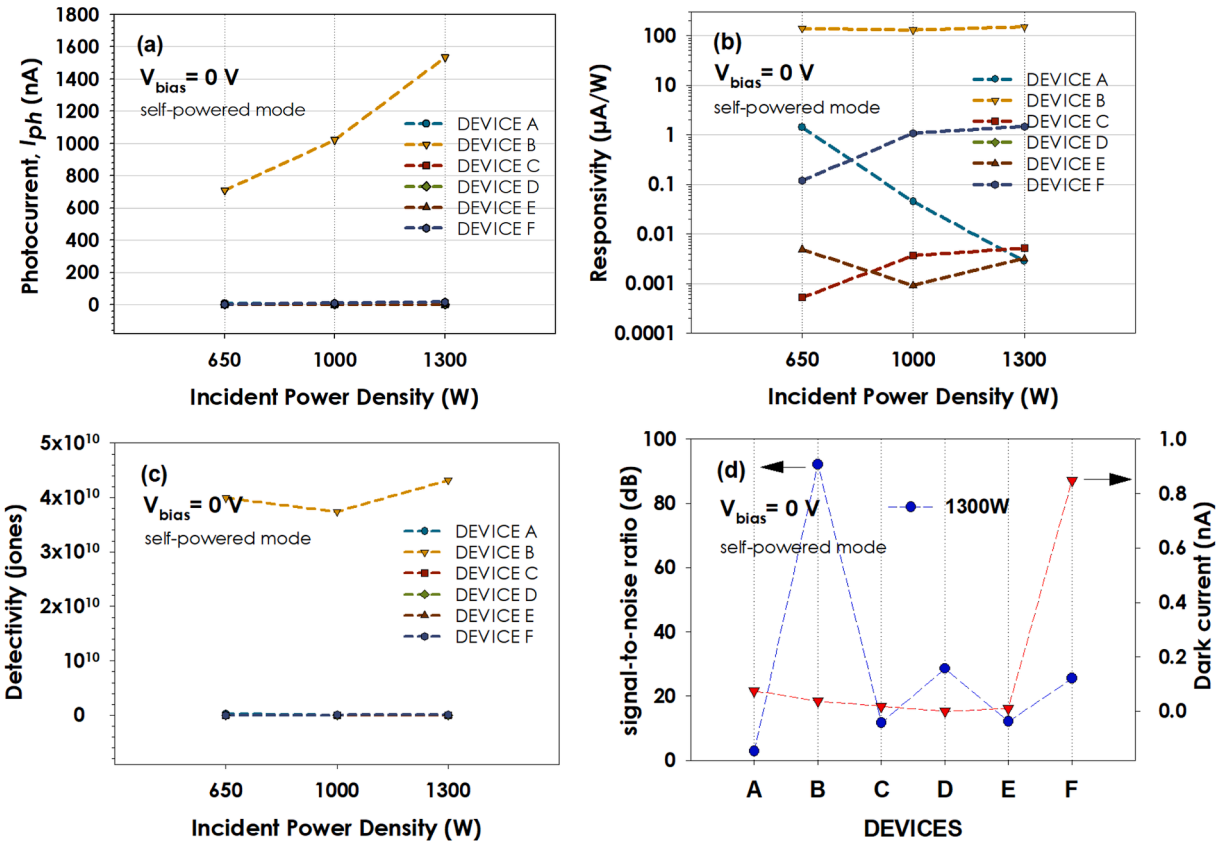

Fig. 8. (a) The PDs' I_{ph}-P curves (b) The PDs' R-P curves. (c) The D* vs P curves (d) The PDs' signal-to-noise ratio and dark current curves at 1300 W; self-powered mode (V_{bias} = 0 V), at UV–vis light intensity.

$3.04x10^5$, 0.011, 0.848nA for each device, respectively. The highest *LDR* values were observed in Device B.

Herein, especially, Device B has higher performance than other devices under incident light intensity. In self-powered mode, theoretically, a *p-i-n* PD generates electrical current through the absorption of photons in the intrinsic layer, which excites electrons from the valence band to the conduction band, creating electron-hole pairs. The built-in electric field at the *p-n* junction drives the photogenerated electrons toward the *n*-type layer and holes toward the *p*-type layer. This drift of charges, facilitated by the electric field, results in a flow of current without any external bias, enabling the PD to function autonomously. The efficiency of this process depends on the thickness of the intrinsic layer and the material quality, making it ideal for applications in sensors and energy harvesting devices where a self-powered operation is crucial. On the other hand, while the fundamental principles of charge generation and movement in *p-n* PDs are similar to those in *p-i-n* PDs, their operational efficiency as self-powered devices can be affected by the structure and spacing of the depletion region. *p-n* PDs can effectively convert light into electrical energy, but they may experience increased recombination losses compared to *p-i-n* structures, especially if the absorption of light occurs primarily in the thicker regions away from the junction. Overall, these factors make the design and material choice critical in optimizing *p-n* PDs for specific applications where self-powered operation is essential [47,48]. In this study, additionally, the fact that Device B in *p-n* PDs has higher PS values than other devices when incident light can be attributed to the design and material choice of the anode contact. A good anode contact minimizes resistance, enhances charge carrier collection efficiency, reduces recombination losses, and ensures stable operation, ultimately leading to better performance characteristics in self-powered mode. On the other hand, it is attributed that the presence of the thicker intrinsic layer (SiO_2) leads to a decrease in the absorption of photons inside and, so, a decrease in the performance of *p-i-n* PDs. While thicker layers may traditionally reduce absorption, the better configuration could be optimized to ensure effective charge carrier collection, leading to improved performance.

Table 2 shows the *R*, *D** and *LDR* values of the fabricated devices and some *p-n* junction devices in self-powered mode. It is seen that the *R* values of Devices A, B and F are high compared to the literature. Especially the *R* value of Device B is relatively high, which is promising in *p-n* based PD applications. It is observed that the *D** of devices A, C, E, and F are low compared to the literature, but the *D** of Device B is at the average value. Consequently, in this study, it has been demonstrated that the same organic semiconductor has exhibited different results in distinct layer and anode contact (Ag and In) configurations. It has also been demonstrated that similar *p-n* and *p-i-n* type heterojunctions have different results in different anode contact configurations in accordance with the theory. These results not only validate the effectiveness of the proposed configurations but also highlight the potential for future applications in sensor technology.

4. Conclusions

The PD characteristics of *p-n* and *p-i-n* vertical structures using different heterostructure configurations, based on *p*-PMIt/*n*-Si, *p*-PMIt/*n*-4HSiC, and *p*-PMIt/*i*-SiO_2/n^{++}-Si are lighted on the confusions of organic–inorganic heterojunction under dark and the UV–Vis various light intensities in this study. Important PD parameter values such as I_o, n, Φ_{Bo}, R_{sh}, and R_s have been shown experimentally and compared with each other. It has been noticed in all devices; I_o values increased due to the increase in the number of minority carriers with increasing light intensity; the highest I_o value was observed in Device F, and the lowest I_o value was observed in Device E. R_s values are showing range from 0.16 to 33.45 kΩ. In contrast, the R_{sh} values range from 0.29 to 33.88 MΩ. At the same time, no meaningful change was observed in R_s values with

Table 2
Comparison of the fabricated devices with R, D^*, and LDR values of p-n junction devices based on some organic semiconductors in literature.

Device	Ma × . R	Ma × . D (Jones)	*LDR* (dB)	Reference
A	1.43 (A/W) @ 650 W/m^2	2.90 × 10^8 @ 650 W/m^2	3.98 × 10^1 @ 650 W/m^2	This work
B	150.4 (A/W) @ 1300 W/m^2	4.32 × 10^{10} @ 1300 W/m^2	9.21 × 10^1 @ 1300 W/m^2	This work
C	0.00053 (A/W) @ 650 W/m^2	2.14 × 10^5 @ 650 W/m^2	1.16 × 10^1 @ 1300 W/m^2	This work
D	7.68 × 10^{-5} (A/W) @ 1300 W/m^2	7.79 × 10^5 @ 1300 W/m^2	2.86 × 10^1 @ 1300 W/m^2	This work
E	0.0049 (A/W) @ 650 W/m^2	2.61 × 10^6 @ 650 W/m^2	1.20 × 10^1 @ 1300 W/m^2	This work
F	1.48 (A/W) @ 1300 W/m^2	8.99 × 10^7 @ 1300 W/m^2	2.55 × 10^1 @ 1300 W/m^2	This work
coronene/CdO	1.52 × 10^{-2} (A/W) @ 20 mW/cm^2	9.94 × 10^9 @ 20 mW/cm^2	–	[33]
ITO/TiO_2/$CsPbBr_3$/SpiroOMeTAD/Au	10.1 × 10^3 (mA/W) @ 405 nm	9.35 × 10^{13}	–	[34]
FTO/Al_2O_3/$CsPbBr_3$/TiO_2/Au	440 mA/W @ 405 nm	1.88 × 10^{13}	–	[29]
Al/CoPOM/*p*-Si	7.38 A/W	2.88 × 10^{10}	–	[35]
WO × /CuPc	7.39 × 10^{-4} (A/W) @ 20 mW/cm^2	6.26 × 10^9	–	[36]
p-WSe_2/n-MoS_2	44 mA.W^{-1}	–	–	[37]
Si-QD/graphene/Si	495 mA.W^{-1}	–	–	[38]
p-WSe_2/*n*-MoS_2	10 mA.W^{-1}	–	–	[39]
W/ZnOseed/ZnO/P_3HT/PEDOT:PSS/AP	156 μA.W^{-1}	0.74 × 10^9	–	[40]
Au/high-*k* CeO_2/*p*-Si	85 A/W @ 910 nm, 0 V bias 1.3 A/W @ 870 nm, 9 V, 600 °C (annealed) 1.2 A/W @ 890 nm, 9 V, 700 °C (annealed)	1.36 × 10^{15}Jones @850 nm 3.79 × 10^{11}Jones @870 nm 1.95 × 10^{11}Jones @ 950 nm	–	[41]
β-Ga_2O_3 nanoflakes/*p*-Si	0.16 mA/W @ 254 nm (UV), 0 V17.1 A/W @ 254 nm (UV), −10 V	–	–	[42]
Al/LiF/NPD/PEDOD:Pss/ITO	0.041	1.43 × 10^9	65.24	[43]
GaN/CoPc	588 mA/W	4.8 × 10^{12}	79.5	[44]
GeSe–$MoTe_2$	52 mA W^{-1}	4.1 × 10^{11}	118	[45]
Au/$NiFe_2O_4$/*p*-Si	0.11A/W @900 nm, 800 °C (annealed) 1.85 A/W @1060 nm, 700 °C (annealed)	5.9 × 10^{14}Jones @1060 nm 9.9 × 10^{13}Jones @1060 nm		[46]

increasing light intensity. According to I-V curves, the asymmetric behavior and electrical conductivity change with increasing light intensity, which is essential for PD applications. The PS properties, a characteristic of UV–visible light intensities, play an essential role in determining light conversion efficiency into electric current for PD applications. In all devices, it was observed that the PS values at reverse bias were higher than the PS values at forward bias, which is an expected behavior for PDs. The R values increased with increasing the voltage under both forward and reverse biases. While increasing light intensity, the R of devices A, B, D, and F increased in the reverse bias, but the R values of devices C and E decreased. Conversely, depending on the supplied voltage, the PS properties of the PDs at UV–vis light intensities were examined. The generated Device B device's PS value in the self-powered mode achieved a maximum at the short-circuit voltage V_{sc} = 0 V. It displayed better photosensitivity behavior, with a minimum value at the open-circuit voltage. Furthermore, the PDs' R and D values were computed. According to the literature, the R and D* values, in this case, declined as power density increased at zero-bias voltage. Additionally, Device B has greater and lower R and D* values than the other devices, respectively.

CRediT authorship contribution statement

Ahmed Ali Alarabi: Writing – original draft, Validation, Formal analysis, Conceptualization. **Osman Çiçek:** Writing – review & editing, Writing – original draft, Supervision, Methodology, Investigation, Formal analysis, Conceptualization. **Hasan Makara:** Data curation. **Fatih Ünal:** Writing – original draft, Formal analysis. **Merve Zurnacı:** Resources. **Şemsettin Altındal:** Writing – review & editing, Supervision.

Declaration of competing interest

The authors declare that they have no known competing financial interests or personal relationships that could have appeared to influence the work reported in this paper.

Acknowledgments

This article is derived from research conducted as part of the first author's doctoral thesis at the Institute of Science, Kastamonu University.

References

[1] A. Basir, et al., Mater. Sci. Semicond. Process. 131 (2021) 105886.
[2] J.Y. Tsao, et al., Adv. Electron. Mater. 4 (1) (2018) 1600501.
[3] V.J. Logeeswaran, et al., IEEE J. Sel. Top. Quantum Electron. 17 (4) (2011) 1002–1032.
[4] S. Demirezen, Y.S. Altındal, Polym. Bull. 77 (1) (2020) 49–71.
[5] R.M. Hewlett, M.A. McLachlan, Adv. Mater. 28 (20) (2016) 3893–9921.
[6] J. Chen, et al., Adv. Funct. Mater. 30 (16) (2020) 1909909.
[7] J.M. Vasquez, et al., J. Phys. D Appl. Phys. 56 (6) (2023) 065104.
[8] H. Yu, et al., Adv. Energy Mater. 11 (9) (2021) 2002646.
[9] A.A. Alarabi, et al., J. Mater. Sci. Mater. Electron. 35 (14) (2024) 957.
[10] W. Ahmad, et al., Appl. Mater. Today 30 (2023) 101717.
[11] G.P. Darshan, et al., Quantum Dots. Woodhead Publishing 1 (2023) 157.

[12] B. Pal, et al., Sol. Energy Mater. Sol. Cells 204 (2020) 110217.
[13] H. Card, E. Rhoderick, J. Phys. D Appl. Phys. 4 (10) (1971) 1589.
[14] M. Zurnacı, et al., New J. Chem. 45 (2021) 22678.
[15] Sze, S.M., Y. Li, and K.K. Ng, Physics of semiconductor devices. 2021: John wiley & sons.
[16] B. Ezhilmaran, et al., J. Mater. Chem. C 9 (19) (2021) 6122.
[17] G. Dushaq, M. Rasras, ACS Appl. Mater. Interfaces 13 (18) (2021) 21499.
[18] A. Schmitz, et al., J. Electron. Mater. 27 (1998) 255.
[19] Hölzl, J. and Schulte, F.K. Work function of metals, in Solid Surface Physics. **1979,** Springer Berlin Heidelberg: Berlin, Heidelberg. p. 1-150.
[20] K.M.A. Saron, et al., Sol. Energy 98 (2013) 485–491.
[21] Z. Xu, et al., J. Appl. Phys. 110 (9) (2011) 093514.
[22] F. Unal, et al., J. Mater. Res. 38 (8) (2023) 2302–2314.
[23] F. Unal, et al., J. Mater. Res. 39 (4) (2024) 675–688.
[24] A. Karabulut, et al., J. Mater. Sci. Mater. Electron. 35 (5) (2024) 362.
[25] Z. Orhan, et al., JOM 74 (8) (2022) 3091–3102.
[26] K. Ganjehyan, et al., Sens. Actuators, A 367 (2024) 115048.
[27] O. Çiçek, et al., Optik 261 (2022) 169137.
[28] R.T. Tung, et al., Mater. Sci. Eng. B 14 (3) (1992) 266–280.
[29] F. Cao, et al., Adv. Funct. Mater. 29 (15) (2019) 1808415.
[30] D. Kaur, M. Kumar, Adv. Opt. Mater. 9 (9) (2021) 2002160.
[31] A. Patel, et al., Superlattice. Microst. 130 (2019) 160–167.
[32] B. Gündüz, et al., Synth. Met. 184 (2013) 73–82.
[33] F. Unal, et al., J. Mater. Sci. Mater. Electron. 33 (33) (2022) 25304–25317.
[34] H. Sun, et al., Adv. Mater. 30 (21) (2018) 1706986.
[35] Yıldırım, M., et al. Advanced Materials Interfaces **2022**:2102304.
[36] S. Aktas, et al., Opt. Mater. 138 (2023) 113709.
[37] R. Cheng, et al., Nano Lett. 14 (10) (2014) 5590–5597.
[38] T. Yu, et al., Adv. Mater. 28 (24) (2016) 4912–4919.
[39] J.H. Yu, et al., Nano Lett. 15 (2) (2015) 1031–1035.
[40] X. Du, et al., Nano Energy 92 (2022) 106694.
[41] S. Godavarthi, et al., Ceram. Int. 50 (18) (2024) 31845–31858.
[42] A. Atilgan, et al., Mater. Today Commun. 24 (2020) 101105.
[43] H. Alzahrani, et al., Synth. Met. 278 (2021) 116830.
[44] Y. Xiao, et al., Nanomaterials 9 (9) (2019) 1198.
[45] N. Zhang, et al., Adv. Mater. Interfaces 9 (15) (2022) 2200150.
[46] N.K.R. Nallabala, et al., Mater. Sci. Semicond. Process. 156 (2023) 107266.
[47] B.E.A. Saleh, M.C. Teich, Fundamentals of photonics, John Wiley & Sons (2019).
[48] D.A. Neamen, D. Biswas, Semiconductor physics and devices, McGraw-Hill higher education, New York, 2011.